Influence of ZnO/graphene nanolaminate periodicity on their structural and mechanical properties

Igor Iatsunskyi, Margarita Baitimirova, Emerson Coy, Luis Yate, Roman Viter, Arunas Ramanavicius, Stefan Jurga, Mikhael Bechelany, Donats Erts

Influence of ZnO/Graphene nanolaminate periodicity on their structural and mechanical properties

Igor Iatsunskyi[1,*], Margarita Baitimirova[2], Emerson Coy[1], Luis Yate[3], Roman Viter[2], Arunas Ramanavicius[4], Stefan Jurga[1], Mikhael Bechelany[5,*], Donats Erts[2,*]

[1]NanoBioMedical Centre, Adam Mickiewicz University, 85 Umultowska str., 61-614, Poznan, Poland

[2]Institute of Chemical Physics, and Institute of Atomic Physics and Spectroscopy, University of Latvia, 19 Raina Boulevard, LV 1586 Riga, Latvia

[3]Surface Analysis and Fabrication Platform, CIC biomaGUNE, Paseo Miramón 182, 20009 Donostia-San Sebastian, Spain

[4]State Research Institute Center for Physical Sciences and Technology, Savanoriu ave. 231, LT-01108 Vilnius, Lithuania

[5]Institut Européen des Membranes, IEM – UMR 5635, ENSCM, CNRS, Univ Montpellier, Montpellier, France

* Corresponding authors. Ph.D.; *E-mail address:* yatsunskiy@gmail.com (I. Iatsunskyi)

Prof., *E-mail address:* donats.erts@lu.lva (D. Erts)

Ph.D.; *E-mail address:* mikhael.bechelany@umontpellier.fr (M. Bechelany)

Structural, electronic and mechanical properties of ZnO/Graphene (ZnO/G) nanolaminates fabricated by low temperature atomic layer deposition (ALD) and chemical vapor deposition (CVD) were investigated. We performed scanning and transmission electron microscopy (SEM/TEM), X-ray diffraction (XRD), electron energy loss spectroscopy (EELS), Raman spectroscopy, X-Ray photoelectron spectroscopy (XPS) and nanoindentation to characterize the ZnO/G nanolaminates. The main structural and mechanical parameters of ZnO/G nanolaminates were calculated. The obtained results were analyzed and interpreted taking into account mechanical interaction and charge effects occurring at the G-ZnO interface. The influence of graphene sublayers number on the mechanical behavior of the ZnO/G nanolaminates was studied. By reducing the bilayer thickness, the mechanical parameters of the films can be tuned

(Young's modulus 100-200 GPa, hardness 3-9 GPa). The softer response of the multilayers as compared to the single layers of ZnO and graphene was attributed to the structural changes in the ZnO layer and the interfaces. This study shows the mechanical behavior of ZnO/G nanolaminates and their influence on the development of novel electro-optical devices based on these structures.

***Keywords*:** Nanolaminate; Graphene; ZnO; XPS; Nanointendation; Multilayers; Atomic layer deposition; Chemical vapor deposition.

1. Introduction

Semiconductor nanolaminates - composite films formed by a number of alternating layers, have recently attracted attention due to their unique electrical, optical and mechanical properties [1]. Among all materials, the composition of zinc oxide (ZnO) and graphene (G) has been extensively studied because of their unique physical properties [2–4]. Graphene is two-dimensional semi-metal for potential applications in nanoelectronics [5], and spintronics [6], due to such properties fast carrier transfer, excellent mechanical stability, and high surface area. On the other hand, ZnO is well-known n-type semiconductor which is broadly used in optoelectronics [7], and sensors [8]. The combination of ZnO and graphene is highly promising for applications in photocatalysis [9,10], optoelectronics [11,12], gas sensors [13], and biosensors [14].

Until now, most of the studies on ZnO/G nanocomposites are focused on the homogeneous dispersion of graphene inside the metal oxide matrix. The distribution of graphene in these nanocomposites is mostly random, which is unfavorable for some applications where the anisotropy of physical properties has some advantages. In this case, the laminated structure of ZnO/G nanocomposite must be used. However, it is still a significant challenge to produce such nanolaminates by alternately deposition of ZnO films and transferring monolayer graphene onto the ZnO-deposited substrate. There are only few researches dedicated to fabrication and investigation of ZnO/G nanolaminates and/or superlattices. *Dusza et al*. have shown that graphene transfer on ZnO, which was obtained by decomposition of $Zn(AcAc)_2$ and spin-coating technique, can be successfully applied in the fabrication of ultra-thin and large area photodetector structures [4]. *Zhu et al.* have demonstrated a room-temperature tunable Raman lasing in a ZnO–graphene superlattice synthesized by using a spatially confined reaction method

[2]. In our previous work [15], ZnO/G nanolaminates were developed by combination of Chemical Vapor Deposition (CVD) and Atomic Layer Deposition (ALD), as one of the most powerful methods for nanolaminates fabrication techniques.[15] We have shown that the number of alternating graphene sublayers and the thickness of ZnO interlayers influenced the structure and the optical properties of the fabricated nanolaminates. Based on the Raman spectroscopy investigation, we concluded that charge transfer from ZnO to graphene occurs during the fabrication process.

Despite some publications dedicated to the optical properties and the application of ZnO/G nanolaminates, further studies are still required. There is still no information about the mechanisms on how the structure of ZnO/G nanolaminates will affect the optical, electronic and mechanical properties. The mechanical behavior of ZnO/G nanolaminates also needs to be established because this finding could play a key role in the development of novel electro-optical devices based on these structures.

Mechanical studies on nanolaminates are mostly focused on elastic modulus and hardness [1,16]. It was shown that mechanical properties of the nanolaminates can be defined by multiple interactions of interfaces in multilayers, but not by the contribution of each individual layer [16]. *Homola et al*. have shown that Al_2O_3/ZnO nanolaminates can improve the mechanical properties of the films due to crystal size reduction, controlled by layer thickness [17]. Several studies have shown that multilayered thin films can be harder [1], or softer [18], than their constituent components. This enables to tailor mechanical properties of composite films for specific applications (e.g. membranes, MEMS) where it is important to predict material behavior at the nanoscale.

In the present research, ZnO/G nanolaminates (with a total thickness of 100 nm) with different number of graphene sublayers were fabricated, and their structural, electronic properties and mechanical parameters were determined as a function of the number of graphene sublayers. Structural, chemical and electronic properties of the fabricated nanolaminates were investigated by means of X-ray, Raman spectroscopy, scanning and transmission electron microscopy, and X-ray photoelectron spectroscopy (XPS). The influence of graphene sublayers number on the mechanical behavior of the ZnO/G nanolaminates was studied by nanowear tests.

2. Experimental

2.1. Fabrication of ZnO/Graphene nanolaminates

ZnO/G nanolaminates were deposited on Si substrates with native silicon oxide (SiO_2) layer. Before deposition, Si substrates were ultrasonically cleaned with acetone, ethanol, and deionized water. High quality single layer graphene was synthesized by Chemical Vapor Deposition (CVD reactor FirstNano EasyTube 101) on previously electrochemically polished and annealed copper foil. Graphene was grown using a gas mixture of 35 sccm (sccm=standard cubic centimeters per minute) methane and 20 sccm hydrogen at 1000 °C temperature and 0.5 Torr pressure. Then, graphene monolayers were transferred to the substrate by polymer-assisted transfer technique followed by the deposition of ZnO layer over graphene according to a previously described technique [15]. All ALD experiments were carried out in a home-built cross-flow reactor, described elsewhere [19]. The ALD of ZnO process was based on DiethyZinc (DEZ) as precursor and water as co-reactant at a deposition temperature of 100°C. Briefly, the process consisted of 0.2s pulse DEZ, 30 s exposure, 40 s purge with Argon, 2 s water pulse, 30 s exposure 40 s purge with Argon to finish the cycle. Schematic diagram of the ZnO/G nanolaminate fabrication process is depicted in Fig. 1. ZnO layers of 10, 25, 50 and 100 nm thickness were deposited by ALD method. The sequential deposition of ZnO layer and graphene transfer was repeated until a multilayer structure with a total thickness of 100 nm was obtained. The samples are named by the formula ZnO*y*G*x*, where *x* is the number of graphene layers and *y* is the thickness in nanometers of ZnO single layer in multilayer structure (Table 1).

2.2. Characterization and mechanical testing of ZnO/Graphene nanolaminates

The morphology and structure of ZnO/G nanolaminates were studied by X-ray diffraction using XRD diffractometer Bruker D5000 (Karlsruhe, Germany). XRD was performed with Cu Kα radiation, using the Bragg-Brentano symmetric configuration. High-resolution transmission electron microscopy with electron energy loss spectroscopy (EELS) was performed by high resolution TEM (HRTEM), JEOL ARM 200F from JEOL (Tokyo, Japan) (200 kV). The cross sections and lamellas for TEM investigations were prepared by focused ion beam milling with JEOL JIB-4000 from JEOL (Tokyo, Japan) by the method described elsewhere [1]. Raman scattering measurements were performed using a Renishaw micro-Raman spectrometer equipped with a confocal microscope Leica (Jena, Germany). The Raman scattering spectra were excited by a 514 nm laser. The beam was focused on the samples with a 50× microscope objective with a numerical aperture of 0.4. X-ray photoelectron spectroscopy (XPS) was performed with a SPECS Sage HR 100 spectrometer from SPECS GmbH (Berlin, Germany), which was equipped

with a non-monochromatic X-ray source (AlK_α line of 1486.6 eV energy) at 300 W and calibrated using the $3d_{5/2}$ line of Ag with a full width at half maximum (FWHM) of 1.1 eV. The selected resolution for the high-resolution spectra was 15 eV of Pass Energy and 0.15 eV/step. All measurements were made in an ultra-high vacuum (UHV) chamber at a pressure around 8×10^{-8} mbar. In order to obtain a depth profile composition, the samples were etched with a 3 kV Ar^+ beam at several times.

Nanohardness and elastic modulus of the samples were measured by the nanoindentation system Hysitron TI 950 Tribo Indenter from Hysitron (Minneapolis, USA) using a Berkovich diamond indenter at maximum load of 10000 μN. Hardness and elastic modulus values were determined from the load-displacement curves by the Oliver-Pharr method [20,21]. Samples were measured for 15 times using the partial unloading function, using a similar procedure as the one described before for very thin layers [16]. Nanowear measurements were performed in the same triboindenter, using a contact load of 100 μN on a 5 μm × 5 μm area. The amount of displaced material was calculated on Gwyddion software from the SPM scan of the tested area [22].

3. Results and Discussion

3.1. Morphology and phase composition

To study the crystalline structure of the ZnO/G nanolaminates, Raman spectroscopy and Grazing Incidence X-ray Diffraction (GIXRD) have been used. The crystallinity and orientation of ZnO layer were investigated by GIXRD, as shown in Fig. 2. The diffraction peaks at 2θ = 31.8º, 34.5º, 36.1º and 56.3º are ascribed to ZnO (100), (002), (102) and (110) crystal planes of the hexagonal Wurtzite structure of ZnO, respectively (JCPDS 65-3411). The peak at 32.9º is corresponding to Si (400). Peaks related to any impurities (e.g. PMMA, Cu, $FeCl_3$) were not observed. It is seen that the ZnO/G nanolaminates with different numbers of graphene layers exhibit similar GIXRD patterns. However, the intensity of the (002) diffraction peak significantly increased for nanolaminates with higher number of graphene layers and decrease of thickness of individual layers, what indicates a preferential growth direction for ZnO layer. This implies that the crystal quality is improved with increasing the number of graphene layers. As was previously shown, the graphene sublayers promote growth of a ZnO layer in [002] direction because of very low mismatch between the graphene and the ZnO (002) hexagonal lattices [15].

In order to determine the phase, graphene quality and to evaluate possible strain and charging effects of obtained nanolaminates we also used μ-Raman spectroscopy as a very sensitive method suitable for local investigations. The Raman spectra of ZnO/G nanolaminates on a SiO_2/Si substrate are shown in Fig. 3. Three main peaks centered at around 1350, 1585 and 2710 cm^{-1}, corresponding to the D, G and 2D modes are observed [23]. The G peak corresponds to in-plane vibrations and the 2D peak is the result of a double resonant process. The shape and the relative intensity of the 2D mode confirm the one-layer structure of graphene in nanolaminates. The D-mode is caused by disordered structure of graphene [24]. Its relative intensity becomes higher with increasing the number of graphene layers. It is well known that the ratio of the intensities (I_D/I_G) provides a sensitive measure of the disorder and crystalline size of the graphene layers [23]. The distinctive increase in the peak intensity ratio I_D/I_G for the samples with higher number of graphene layers indicates the growing of defects concentration. This is due to the structural damage caused by the graphene transferring and ALD process [15]. Another peaks, which are the D+D' (∼2920 cm^{-1}) and D+D''(∼2460 cm^{-1}) bands, are combinations of phonons with different momenta, thus requiring a defect for its activation [25].

It is seen that the graphene mode is split into two peaks, G-peak (∼1585 cm^{-1}) and D'-peak (∼1615 cm^{-1}) (Fig. 3). This splitting is explained by randomly distributed impurities or surface charges in the graphene (Baitimirova *et al*>, 2016). The main reason is that the localized vibrational modes of the impurities can interact with the extended phonon modes of graphene resulting in the observed splitting. However, in our previous publication, we have shown that the main reason of G-mode splitting is a charging effect which is attributed to the negative charge of graphene by electron transfer from ZnO layer [15]. It was also shown that this electron transfer leads to the formation of depletion layer in ZnO layer and facilitates accumulations of holes in it. Abovementioned electronic model allowed us to explain some optical properties in fabricated ZnO/G nanolaminates [15]. However, in order to prove this model and its affecting on electronic properties of ZnO/G nanolaminates, more suitable experimental techniques (XPS, UPS etc.) should be applied (shown later in this manuscript).

Fig. 4 shows the cross-sectional TEM and SEM images of the ZnO/G nanolaminates. TEM results indicate that the ZnO/G nanolaminates are well prepared by combination of ALD and CVD. It is clearly seen that the individual layers of ZnO and graphene are of constant thickness and reproducible. The total thickness of all obtained ZnO/G nanolaminates is about 100 nm. The

increase of a number of graphene interlayers leads to the increase of nanolaminate surface roughness (SI, Fig. S1). This result was also confirmed by AFM measurements (SI, Fig. S1 and S2). As a consequence the highest roughness is observed for the ZnO10G11 sample (Fig. 4f). The crystalline structure of the ZnO layer was characterized by HRTEM and fast Fourier transform (FFT) (Fig. 4b). HRTEM and FFT analysis of ZnO/G nanolaminates showed the presence of (100), (002), (101), (110), and (103) fringes corresponding to plane of Wurtzite crystal structure of ZnO (Fig. 4b).

To identify the nature of the interfacial layer, EELS elemental mapping of the ZnO/G nanolaminates were acquired (SI, Fig. S3). A clear interface between the ZnO and graphene can be observed from the EELS elemental mapping, as shown in supplementary information (Fig. S3).

3.2. XPS analysis

To determine the chemical composition of the surface we used XPS analysis. The survey spectra for the ZnO/G nanolaminates are shown in Fig. 5a with the core level peaks of Zn 3d, Zn 3p, Zn 3s, Zn 4s, C 1s, O 1s, and Auger peaks Zn LMM, O KLL and C KLL identified. The main Auger peak (LMM) of the Zn occurs at kinetic energy (Ek) about 988 eV. As was shown in our previous works, the modified Auger parameter (Ek(LMM)+BE(Zn $2p_{3/2}$)) is a useful tool for determination of stoichiometry and phase of the obtained structures [26]. The calculated modified Auger parameters yielded a value of 2009.7±0.2 eV for all samples [27]. This indicates the formation of stoichiometric ZnO. This result is in agreement with the TEM and XRD. Analysis of the first derivative of the C KLL Auger peak and the subsequent calculation of the D-parameter (the energy separation between maxima and minima in the first derivative of the C KLL Auger peak) revealed sp^2 carbon (SI, Fig. S3) [28].

The Zn 2p core-level XPS spectrum shows doublet spectral lines at about binding energies of 1022±0.2 eV (Zn $2p_{3/2}$) and 1045±0.2 eV (Zn $2p_{1/2}$), respectively. The spin-orbit splitting of Zn 2p for ZnO layer (sample ZnO100G0) is 23.1 eV, which coincides with the results for Zn^{2+} in ZnO (Iatsunskyi *et al*>, 2017). Regarding oxygen, the main peak is centered at about 531 eV, in agreement with the position expected for O in ZnO lattice [30]. The typical O 1s peak of ZnO can be fitted into minimum two Gaussian peaks, as suggested earlier [29]. The higher binding energy peaks located at 532.5 eV should be assigned to hydroxyl groups which are always

observed for ZnO layers fabricated by ALD, whereas the lower binding energy of 531 eV is attributed to the O^{2-} ion (Zn–O bonding) in the Wurtzite structure of hexagonal ZnO [29].

It is seen that an increase in the number of graphene sublayers in ZnO/G nanolaminates leads to the shift to higher BEs of the main O 1s component and the decrease of Zn 2p spin–orbit splitting to 23 eV value. This phenomenon could be explained by the charging effects at the interface [31]. This finding completely confirms our previous assumption about the charging effects.

A number of components can be identified for C 1s core levels (SI, Fig. S4)– C-C sp^2 (284.2±0.1 eV), C-O (285.5±0.1 eV), C=O (287.1±0.1 eV), and O=C-O (288.6±0.1 eV) [32]. XPS spectra clearly indicate a graphene on the surface of ZnO/G nanolaminates. For all samples the relative concentration of C sp^2 in graphene and other functional groups remain almost the same.

3.3. Nanointendation tests

Nanoindentation tests were performed in order to investigate the mechanical response of the samples as a function of the number of graphene sublayers. The reported mechanical values of ZnO layers vary from the techniques used, from sputtering layers E=154 and H=8.7 GPa [33], Pulsed laser deposition E=117-212 GPa and H=5.9-11.5 GPa, depending on their crystalline orientation [34], and ALD with E=125 GPa and H=5.6 GPa [35]. In the case of multilayers, it is known that the increment of interfaces results in higher hardness and elastic constant of the samples, however this is true for crystalline samples in which the interfaces allow the allocation of shear stress, which stops the propagation of fractures and, ultimately, prevents the failure of the films [16,36–38]. Nevertheless, the increment of multilayers also increases stresses which can lead to delamination of the films. However, this is not likely to take place in our samples, due to the mixed fabrication method used in the preparation of the samples, which in principle presents almost stress free interfaces, between graphene and ZnO layer. Nevertheless, the mechanical stability of the samples is expected to decrease as a function of the graphene interlayers, this is due to poor mechanical contact between transferred graphene and growing ZnO layer, which is worsening by the repetition of the process as clearly shown in Fig. 4. Mechanical results are collected in Fig. 6, notice the high mechanical response of the ZnO100G2 sample, which yields mechanical values comparable to those reported by other techniques in the literature [39]. The decrement of mechanical properties observed for 3, 5 and 6 bilayers is

attributed to in-homogeneity of the interfaces and the pseudo delimitative behavior promoted by the indenter. However, the mechanical response can be attributed to the progressive reduction in grain size, due to the increment of graphene layers. Moreover, it is important to highlight that the mechanical response of the 6 bilayers sample, which, although described here as the one with softer properties, falls well within the reported other ZnO thin films, such as: ZnO/6H-SiC (H=5.9±0.2 & E=117.1±0.4 GPa),[40] (E=98.48±5.4 GPa) [41], ZnO/Si(111) (H=6.7 & E=137±3) [18], and c-ZnO (H=5.67±0.9 GPa & E=133.68±10.8) [42], which clearly shows that the whole set of samples, remain strong and mechanically competitive. For comparison, we have also put values of Young's Module (E) and Hardness (H) of pure ZnO layer obtained in our experiments into the Fig. 6. However, as can be seen from the Fig. 6, these values do not match to the general concept of mechanical parameters reducing.

In addition to the previous measurements, the ***H/E*** ratio is evaluated as a quality control of the wear coefficient of the samples. The ***H/E*** ratio is associated with large elastic strain before plastic deformation, thus, it is mainly attributed to the wear resistance of the materials [43,44]. In Fig. 6a inset, the result of ***H/E*** is shown, showing the highest value for ZnO100G2. Furthermore, nanowear tests performed on the samples are shown in Fig. 6b in order to complement the previously presented results. The displaced material increases with the number of layers, showing the accuracy of the H/E ratio and the increased fragility of the samples with the increment of graphene layers.

Finally, although a decrement on mechanical resilience is observed, the obtained values are still in the range of commercial metal oxides and still in a competitive level. More studies are needed in order to determine the role of interface homogeneity, oxides crystallinity and elastic properties of the nanolaminates on the mechanical and tribological aspects of the ZnO/G multilayers.

4. Conclusion

In conclusion, the ZnO/G nanolaminates have been developed and investigated. The structural, electronic and mechanical properties of ZnO/G nanolaminates determined from the XPS, SEM/TEM, Raman spectroscopy, XRD and nanointendation analyses provide an important information about studied properties of ZnO/G nanolaminates. The number of alternating graphene and ZnO interlayers and the thickness of ZnO interlayers influenced the structure,

optical and mechanical properties of the fabricated nanolaminates. It was shown that mechanical properties of ZnO/G nanolaminates are tailored by their structural parameters - the number of graphene sublayers. It was shown that the mechanical stability of ZnO/G nanolaminates decreases as a function of the graphene sublayers because of the poor mechanical contact between transferred graphene and ZnO, which was deposited by ALD method. Comparing these results with those obtained previously (see [15]), we can draw a conclusion that increasing the number of graphene layers affects the mechanical parameters of ZnO/G nanolaminates and their optical (*e.g.* PL) properties due to structural/morphological effects at the interface between ZnO and graphene sublayers. The results are very promising for the advanced use of multilayered graphene structures in various applications where it is important to tune their structural, optical and mechanical properties (e.g. tissue engineering, medical implants etc.).

Acknowledgements

M.B., R.V., and D.E acknowledge support by Latvia National Research Program IMIS 2 and France-Latvia OSMOSE Project no. LV-FR/2017/3. I.I. acknowledges the support from Ministry of Science and Higher Education of Poland by the Polish-Portuguese bilateral project. Authors would like to thank Yasutomo Nishida from JEOL, for his kind collaboration during the preparation of this manuscript.

References

1. I. Iatsunskyi, E. Coy, R. Viter, G. Nowaczyk, M. Jancelewicz, I. Baleviciute, K. Załęski, and S. Jurga, J. Phys. Chem. C **119**, 20591 (2015).

2. H. Zhu, X. Xu, X. Tian, J. Tang, H. Liang, L. Chen, Y. Xie, X. Zhang, C. Xiao, R. Li, Q. Gu, P. Hua, and S. Ruan, Adv. Mater. **29**, 1604351 (2017).

3. X. Men, H. Chen, K. Chang, X. Fang, C. Wu, W. Qin, and S. Yin, Appl. Catal. B Environ. **187**, 367 (2016).

4. M. Dusza, F. Granek, and W. Strek, Opt. Mater. (Amst). 1 (2017).

5. A. Brataas, Nature **452**, 419 (2008).

6. W. Han, R. K. Kawakami, M. Gmitra, and J. Fabian, Nat Nano **9**, 794 (2014).

7. K. C. Pradel, Y. Ding, W. Wu, Y. Bando, N. Fukata, and Z. L. Wang, ACS Appl. Mater. Interfaces **8**, (2016).

8. R. Viter, M. Savchuk, I. Iatsunskyi, Z. Pietralik, N. Starodub, N. Shpyrka, A. Ramanaviciene, and A. Ramanavicius, Biosens. Bioelectron. **99**, 237 (2018).

9. E. Rokhsat and O. Akhavan, Appl. Surf. Sci. **371**, 592 (2016).

10. L. Zhang, L. Du, X. Yu, S. Tan, X. Cai, P. Yang, Y. Gu, and W. Mai, ACS Appl. Mater. Interfaces **6**, 3623 (2014).

11. M. Yu, A. Wang, Y. Wang, C. Li, and G. Shi, Nanoscale **6**, 11419 (2014).

12. B. J. Moon, K. S. Lee, J. Shim, S. Park, S. H. Kim, S. Bae, M. Park, C. L. Lee, W. K. Choi, Y. Yi, J. Y. Hwang, and D. I. Son, Nano Energy **20**, 221 (2016).

13. H. Zhang, Y. Cen, Y. Du, and S. Ruan, Sensors (Switzerland) **16**, (2016).

14. F. Liu, Y. Zhang, J. Yu, S. Wang, S. Ge, and X. Song, Biosens. Bioelectron. **51**, 413 (2014).

15. M. Baitimirova, R. Viter, J. Andzane, A. van der Lee, D. Voiry, I. Iatsunskyi, E. Coy, L. Mikoliunaite, S. Tumenas, K. Załęski, Z. Balevicius, I. Baleviciute, A. Ramanaviciene, A. Ramanavicius, S. Jurga, D. Erts, and M. Bechelany, J. Phys. Chem. C **120**, 23716 (2016).

16. E. Coy, L. Yate, Z. Kabacińska, M. Jancelewicz, S. Jurga, and I. Iatsunskyi, Mater. Des. **111**, 584 (2016).

17. T. Homola, V. Buršíková, T. V. Ivanova, P. Souček, P. S. Maydannik, D. C. Cameron, and J. M. Lackner, Surf. Coatings Technol. **284**, 198 (2015).

18. R. Raghavan, M. Bechelany, M. Parlinska, D. Frey, W. M. Mook, A. Beyer, J. Michler, and I. Utke, Appl. Phys. Lett. **100**, 191912 (2012).

19. J. A. Whitby, F. Östlund, P. Horvath, M. Gabureac, J. L. Riesterer, I. Utke, M. Hohl, L. Sedláček, J. Jiruše, V. Friedli, M. Bechelany, and J. Michler, Adv. Mater. Sci. Eng. **2012**, (2012).

20. W. Oliver and G. Pharr, J. Mater. Res. **7**, 1564 (1992).

21. W. C. Oliver and G. M. Pharr, J. Mater. Res. **19**, 3 (2004).

22. D. Nečas and P. Klapetek, Open Phys. **10**, 181 (2012).

23. A. C. Ferrari, J. C. Meyer, V. Scardaci, C. Casiraghi, M. Lazzeri, F. Mauri, S. Piscanec, D. Jiang, K. S. Novoselov, S. Roth, and A. K. Geim, Phys. Rev. Lett. **97**, (2006).

24. L. M. Malard, M. A. Pimenta, G. Dresselhaus, and M. S. Dresselhaus, Phys. Rep. **473**, 51 (2009).

25. J. Hong, M. K. Park, E. J. Lee, D. Lee, D. S. Hwang, and S. Ryu, Sci. Rep. **3**, 2700 (2013).

26. I. Iatsunskyi, M. Kempiński, G. Nowaczyk, M. Jancelewicz, M. Pavlenko, K. Załeski, and S. Jurga, Appl. Surf. Sci. **347**, 777 (2015).

27. L. S. Dake, D. R. Baer, and J. M. Zachara, Surf. Interface Anal. **14**, 71 (1989).

28. S. Kaciulis, A. Mezzi, P. Calvani, and D. M. Trucchi, Surf. Interface Anal. **46**, 966 (2014).

29. I. Iatsunskyi, A. Vasylenko, R. Viter, M. Kempiński, G. Nowaczyk, S. Jurga, and M. Bechelany, Appl. Surf. Sci. **411**, 494 (2017).

30. R. Al-Gaashani, S. Radiman, a. R. Daud, N. Tabet, and Y. Al-Douri, Ceram. Int. **39**, 2283 (2013).

31. R. Viter, I. Iatsunskyi, V. Fedorenko, S. Tumenas, Z. Balevicius, A. Ramanavicius, S. Balme, M. Kempin, G. Nowaczyk, S. Jurga, and M. Bechelany, J Phys Chem C **120**, 5124−5132 (2016).

32. a V Shchukarev and D. V Korolkov, Cent. Eur. J. Chem. **2**, 347 (2004).

33. R. Navamathavan, K.-K. Kim, D.-K. Hwang, S.-J. Park, J.-H. Hahn, T. G. Lee, and G.-S.

Kim, Appl. Surf. Sci. **253**, 464 (2006).

34. S.-R. Jian, I.-J. Teng, P.-F. Yang, Y.-S. Lai, J.-M. Lu, J.-G. Chang, and S.-P. Ju, Nanoscale Res. Lett. **3**, 186 (2008).

35. K. Tapily, D. Stegall, D. Gu, H. Baumgart, G. Namkoong, and A. A. Elmustafa, ECS Trans. **25**, 85 (2009).

36. Z. Shafiee, M. E. Bahrololoom, and B. Hashemi, Mater. Des. **108**, 19 (2016).

37. L. Chen and Y. X. Xu, Mater. Des. **106**, 1 (2016).

38. A. Dück, N. Gamer, W. Gesatzke, M. Griepentrog, W. Österle, M. Sahre, and I. Urban, Surf. Coatings Technol. **142**–**144**, 579 (2001).

39. S.-R. Jian, J. Alloys Compd. **494**, 214 (2010).

40. S. R. Jian, I. J. Teng, P. F. Yang, Y. S. Lai, J. M. Lu, J. G. Chang, and S. P. Ju, Nanoscale Res. Lett. **3**, 186 (2008).

41. V. Bhardwaj, R. Chowdhury, and R. Jayaganthan, Appl. Surf. Sci. **389**, 1023 (2016).

42. V. Bhardwaj, R. Chowdhury, and R. Jayaganthan, J. Mater. Res. **32**, 1432 (2017).

43. J. Guo, H. Wang, F. Meng, X. Liu, and F. Huang, Surf. Coatings Technol. **228**, 68 (2013).

44. A. V. Pshyk, L. E. Coy, L. Yate, K. Załęski, G. Nowaczyk, A. D. Pogrebnjak, and S. Jurga, Mater. Des. **94**, 230 (2016).

Figures and table captions

Table 1. Samples description

Fig. 1. Schematic diagram of the fabrication of ZnO/Graphene nanolaminates.

Fig. 2. GIXRD patterns of ZnO/Graphene nanolaminates

Fig. 3. Raman spectra of ZnO/Graphene nanolaminates

Fig. 4. SEM/TEM images of cross-section of ZnO/Graphene nanolaminates: (a) ZnO100G2 sample, (inset - high magnification of white square); (b) the interface between Si-Graphene-ZnO (inset - FFT of yellow square); (c) ZnO50G3 sample; (d) ZnO25G5 sample; (e) ZnO20G6 sample; f) ZnO10G11 sample.

Fig. 5. (a) XPS survey spectra of the ZnO/Graphene nanolaminates; XPS core-level spectra of (b) Zn 2p, and (c) O 1s.

Fig. 6. (a) Values of elastic modulus E (left axis) and hardness H (right axis) *vs* the number of graphene layers for ZnO/Graphene nanolaminates and values of 100 nm ZnO layer (marked by red/black squares). The inset shows the value of H/E *vs* the number of graphene layers. Sketch shows the piling up effect of defects and delamination's as the number of layers increases, (b) Topographic images resulting of nanowear experiments.

Table 1. Samples description

Samples	ZnO layer thickness nm	Number of ZnO layers	Number of Gr layers
ZnO100G0	100	1	0
ZnO100G2	100	1	2
ZnO50G3	50	2	3
ZnO25G5	25	4	5
ZnO20G6	20	5	6
ZnO10G11	10	10	11

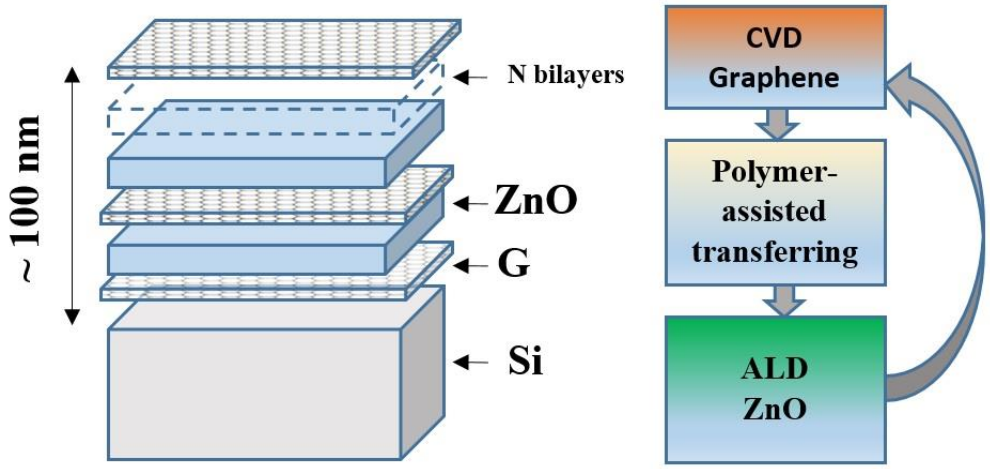

Fig. 1. Schematic diagram of the fabrication of ZnO/Graphene nanolaminates.

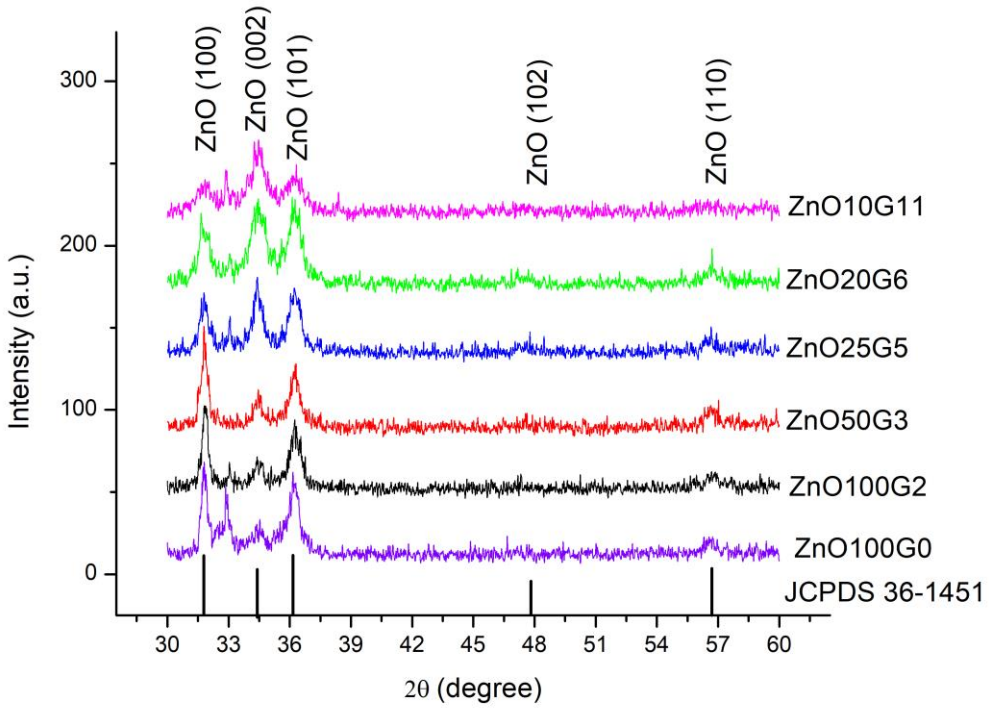

Fig. 2. GIXRD patterns of ZnO/Graphene nanolaminates

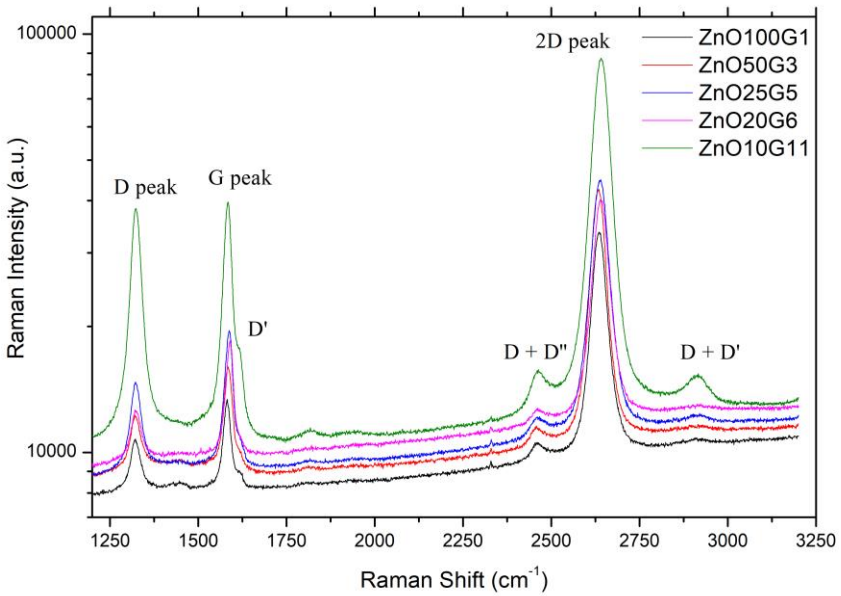

Fig. 3. Raman spectra of ZnO/Graphene nanolaminates

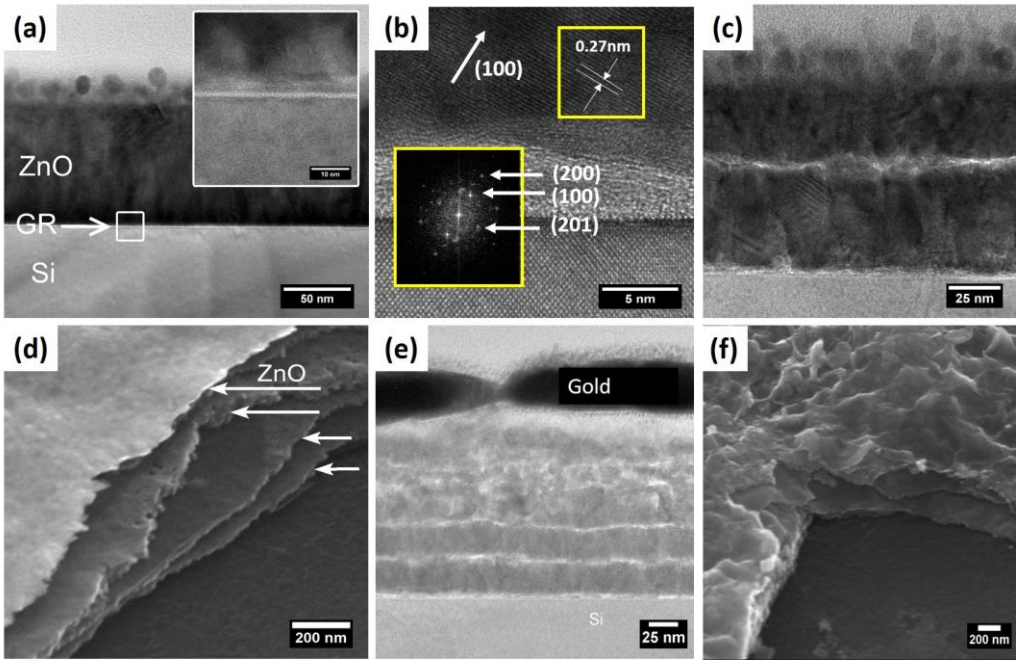

Fig. 4. SEM/TEM images of cross-section of ZnO/Graphene nanolaminates: (a) ZnO100G2 sample, (inset - high magnification of white square); (b) the interface between Si-Graphene-ZnO (inset - FFT of yellow square); (c) ZnO50G3 sample; (d) ZnO25G5 sample; (e) ZnO20G6 sample; f) ZnO10G11 sample.

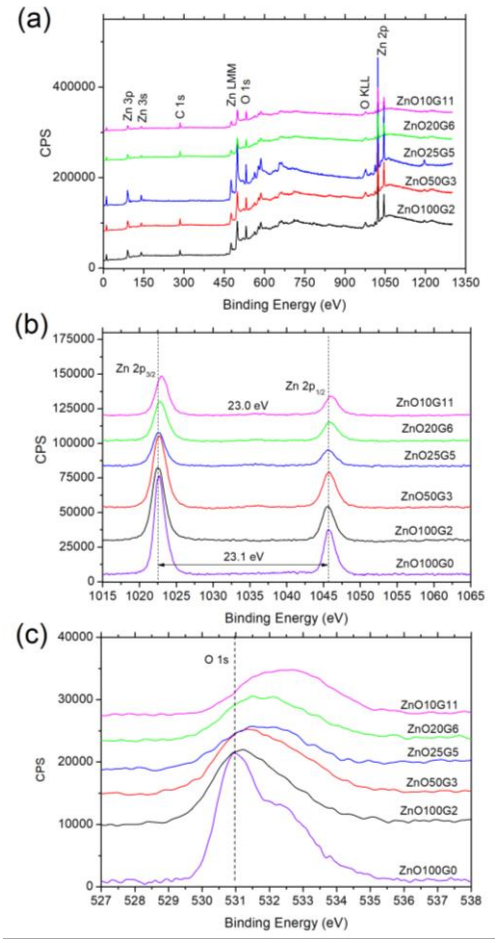

Fig. 5. (a) XPS survey spectra of the ZnO/Graphene nanolaminates; XPS core-level spectra of (b) Zn 2p, and (c) O 1s.

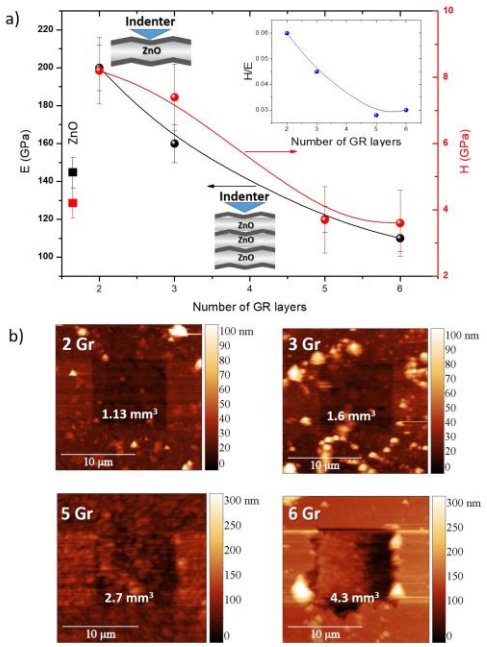

Fig. 6. (a) Values of elastic modulus E (left axis) and hardness H (right axis) *vs* the number of graphene layers for ZnO/Graphene nanolaminates and values of 100 nm ZnO layer (marked by red/black squares). The inset shows the value of H/E *vs* the number of graphene layers. Sketch shows the piling up effect of defects and delamination's as the number of layers increases, (b) Topographic images resulting of nanowear experiments.